Electronic Supplementary Information (ESI) for:

Copper-zinc oxide interface as a methanol-selective structure in Cu-ZnO catalyst during catalytic hydrogenation of carbon dioxide to methanol

Saeed Saedy[a,1,], Mark A. Newton[b], Maxim Zabilskiy[a], Jin Hee Lee[a,2], Frank Krumeich[c], Marco Ranocchiari[a], Jeroen A. van Bokhoven[a,b,*]*

a) Laboratory for Catalysis and Sustainable Chemistry, Paul Scherrer Institute, 5232 Villigen, Switzerland.

b) Institute for Chemistry and Bioengineering, ETH Zurich, Vladimir-Prelog-Weg 1, 8093 Zürich, Switzerland.

c) Laboratory of Inorganic Chemistry, Institute for Chemical and Bioengineering, ETH Zurich, 8093 Zurich, Switzerland.

[*]Corresponding authors; E-mail address: jeroen.vanbokhoven@chem.ethz.ch , s.saedy@tudelft.nl

[1]Present address: Department of Chemical Engineering, Delft University of Technology, van der Maasweg 9, 2629 HZ Delft, The Netherlands.

[2]Present address: Center for Environment & Sustainable Resources, Korea Research Institute of Chemical Technology, 34114 Daejeon, South Korea.

Calculation of the methanol activity normalized by the surface copper atoms

Calvin et al.[1] derived an equation to determine the coordination number of a particle as a function of its radius (R):

$$N_{nano} = [1 - \frac{3}{4}\left(\frac{r}{R}\right) + \frac{1}{16}(\frac{r}{R})^3]N_{bulk} \quad (1)$$

where r is the average distance between the nearest-neighbor atoms.

The apparent coordination numbers of metal particles obtained from EXAFS analysis are smaller than the actual value for small clusters, and this deviation becomes more significant at elevated temperatures for small particles,[2] especially for low Debye temperature materials such as copper. Clausen et al.[2] demonstrated a linear behavior of the deviation of the apparent coordination number from the actual value, for copper particles up to 7 nm through the use of molecular dynamics simulations. The curve derived by Clausen et al. is employed for correction of apparent coordination numbers. Accordingly, the 1st shell coordination number of PCVD and CA samples were corrected to 9.0 and 8.9, respectively. Also, the 1st shell coordination number of IMP sample was corrected to 8.0.

Then, the average copper particle size were calculated using the corrected coordination numbers and equation (1). As an example, substituting the N_{nano} = 9, N_{bulk} = 12, and r = 2.51 Å for PCVD sample and solving equation (1), results in following:

$$9 = \left[1 - \frac{3}{4}\left(\frac{2.51}{R}\right) + \frac{1}{16}\left(\frac{2.51}{R}\right)^3\right]12 \rightarrow R_1 \approx -0.7\ \text{Å}, R_2 \approx 0.8\ \text{Å}\ and\ R_3 \approx 7.5\ \text{Å}$$

Among the obtained values, 7.5 Å is physically meaningful. Hence, the average diameter of copper particles in PCVD sample can be estimated about 15 Å (1.5 nm). In the same way, the average size of copper particles in the CA and IMP samples is estimated to be ca. 14.4 Å and 11 Å, respectively. It is worth to note that the average particle size obtained for CA sample is similar to the observed particle size using HAADF-STEM images (**Figure S5**). In the case of PCVD and IMP samples, we cannot use the STEM images for validation, since we are not able to differentiate the copper and zinc oxide particles. The dispersion of copper (D_{Cu}) as function of particle diameter can be calculated using the following relation[3]:

$$D_{Cu} = 6\frac{v_m / a_m}{d} \quad (2)$$

where *d* is the average dimeter of cluster (Å) and for copper v_m=11.83 Å^3 and a_m=6.85 Å^2.

Accordingly, the copper dispersion using equation (2) and the average dimeter calculated using equation (1) can be calculated as follow:

$$D_{Cu\_PCVD} = 6 \times \frac{{}^{11.83}/_{6.85}}{15} = 0.69$$

In the same way, the copper dispersion of CA and IMP samples were estimated about 0.71 and 0.92, respectively.

Accordingly, the methanol activity of the catalysts normalized by the surface copper atoms was calculated by dividing the copper productivity (in $\mu mol \cdot g^{-1}_{Cu} \cdot min^{-1}$) by copper dispersion of each catalyst:

Methanol activity of PCVD catalyst: $\frac{930}{0.69} = 1372\ \mu mol \cdot g^{-1}_{Cu\_surface} \cdot min^{-1}$

In the same way, the activity for methanol production of the catalysts, normalized by the surface copper atoms of CA and IMP samples, were calculated as 288 $\mu mol \cdot g^{-1}_{Cu\_surface} \cdot min^{-1}$ and 865 $\mu mol \cdot g^{-1}_{Cu\_surface} \cdot min^{-1}$, respectively. The methanol productivity of these samples is 200 $\mu mol \cdot g^{-1}_{Cu} \cdot min^{-1}$ and 765 $\mu mol \cdot g^{-1}_{Cu} \cdot min^{-1}$ for CA and IMP catalysts respectively.

The results of calculation of the methanol activity normalized by the surface copper atoms are summarized in **Table S3**.

References

1. Calvin, S.; Miller, M. M.; Goswami, R.; Cheng, S.-F.; Mulvaney, S. P.; Whitman, L. J.; Harris, V. G., Determination of crystallite size in a magnetic nanocomposite using extended x-ray absorption fine structure. *Journal of Applied Physics* **2003,** *94* (1), 778-783.
2. Clausen, B. S.; Grabaek, L.; Topsoe, H.; Hansen, L. B.; Stoltze, P.; Norskov, J. K.; Nielsen, O. H., A New Procedure for Particle Size Determination by EXAFS Based on Molecular Dynamics Simulations. *Journal of Catalysis* **1993,** *141* (2), 368-379.
3. Mestl, G.; Knözinger, H., Characterization of Solid Catalysts: Physical Properties: Structure and Morphology: Vibrational Spectroscopies. In *Handbook of Heterogeneous Catalysis*, 2008; Vol. 2-5, pp 539-574.

Table S1

Table S1. The chemical composition of different $ZnO/Cu/Al_2O_3$ catalysts synthesized in this study.

Sample name	Synthesis method	Zinc deposition time (h)	Impregnated copper wt%	Deposited zinc wt%	Zn:Cu atomic ratio
*CA	impregnation	0	4.7	0	0
CZA1	PCVD	0.5	4.5	0.2	0.05
CZA2	PCVD	1	4.5	0.8	0.18
*PCVD	PCVD	2	4.5	2.2	0.50
CZA3	PCVD	3	4.7	3.3	0.72
CZA4	PCVD	6	4.7	5.2	1.14
CZA5	PCVD	9	4.7	7.5	1.64
* IMP	impregnation	n.a.	4.5	2.2	0.50

* These three samples were named differently from the rest of samples aiming at easier use in the main text.

Table S2

Table S2. The comparison of the methanol performance of PCVD catalyst with an industrial sample.

Catalyst	Process temperature (°C)	Process pressure (bar)	Methanol rate ($\mu mol \cdot g_{Cu}^{-1} \cdot min^{-1}$)	Methanol selectivity (%)
Industrial	260	15	552	48
Industrial	260	50	2020	41
PCVD	250	30	930	65

* Due to different experimental conditions (especially the reaction pressure) and the different compositions of the catalysts, any conclusion cannot be drawn unequivocally.

Table S3

Table S3. The summary of the BET surface area measurements.

	Pristine alumina	CA	PCVD	IMP
BET surface area ($m^2 \cdot g^{-1}$)	142	123	113	106
BJH pore volume ($cm^3 \cdot g^{-1}$)[a]	0.24	0.22	0.20	0.19
BJH average pore width (Å)[b]	61	58	63	57

a. the adsorption volume of pores with the width of 17 - 3000 Å.
b. the adsorption average pore width (4V/A).

Table S4

Table S4. The apparent and corrected 1st shell coordination number of copper nanoparticles, copper nanoparticle diameter, copper dispersion, and methanol activity normalized by the surface copper atoms.

Sample	Apparent 1st shell CN	Corrected 1st shell CN	Average copper particle size (Å)	Copper dispersion	Methanol activity ($\mu mol \cdot g^{-1}_{Cu\_surface} \cdot min^{-1}$)
PCVD	8.0	9.0	15.0	0.69	1372
CA	7.9	8.9	14.4	0.71	288
IMP	6.7	8.0	11.0	0.92	865

Table S5

Table S5: Structural and statistical parameters derived from the fitting of k^3-weighted copper *K*-edge EXAFS for the CA, PCVD, and IMP catalysts; pressurized to15 bar after reduction (at 250°C under 25 vol. % of hydrogen in helium). K_{min}=3, K_{max}=11.5, AFAC =0.9*

Sample	Shell	CN	R (Å)	DW ($2\sigma^2$)	Fitting parameters
CA	Cu-Cu	8.3	2.51	0.031	E_F = -8.4
	Cu-O	n.a.	n.a.	n.a.	R% = 47
PCVD	Cu-Cu	8.5	2.51	0.033	E_F = -7.9
	Cu-O	n.a.	n.a.	n.a.	R% = 44
IMP	Cu-Cu	8	2.50	0.033	E_F = -7.7
	Cu-O	0.7	1.99	0.007	R% = 36

*AFAC: related to the proportion of electrons undergoing scattering post absorption that contribute to the EXAFS.

CN: Coordination number (± 10 % of stated value)

DW: Debye – Waller factor where σ is the root mean square inter-nuclear separation (Å)

EF: Edge position relative to Vacuum zero (Fermi energy, eV)

R(%) (fit agreement factor): $\left(\frac{\int [c^T - c^E]k^3 dk}{[c^E]k^3 dk}\right) \times 100$, where c^T and c^E are the theoretical and experimental EXAFS and k is the photoelectron wave vector.

Table S6

Table S6: Structural and statistical parameters derived from the fitting of k^3-weighted zinc *K*-edge EXAFS for the PCVD and IMP catalysts; pressurized to15 bar after reduction (at 250°C under 25 vol. % of hydrogen in helium). K_{min}=2.5, K_{max}=10.5, AFAC =0.9*

Sample	Shell	CN	R (Å)	DW ($2\sigma^2$)	Fitting parameters
PCVD	Zn-O	2.6	1.9	0.007	E_F = -2.85
	Zn-O	1.5	2.07	0.005	R(%) = 52
	Zn-Zn	0.9	3.16	0.015	
IMP	Zn-O	1.4	1.91	0.015	E_F = -1.5
	Zn-O	2.1	1.97	0.015	R(%) = 55
	Zn-Al	n.a.	n.a.	n.a.	

*AFAC: related to the proportion of electrons undergoing scattering post absorption that contribute to the EXAFS.

CN: Coordination number (± 10 % of stated value)

DW: Debye – Waller factor where σ is the root mean square inter-nuclear separation (Å)

E_F: Edge position relative to Vacuum zero (Fermi energy, eV)

R(%) (fit agreement factor): $\left(\frac{\int [c^T - c^E]k^3 dk}{[c^E]k^3 dk}\right) \times 100$, where c^T and c^E are the theoretical and experimental EXAFS and k is the photoelectron wave vector.

Figure S1

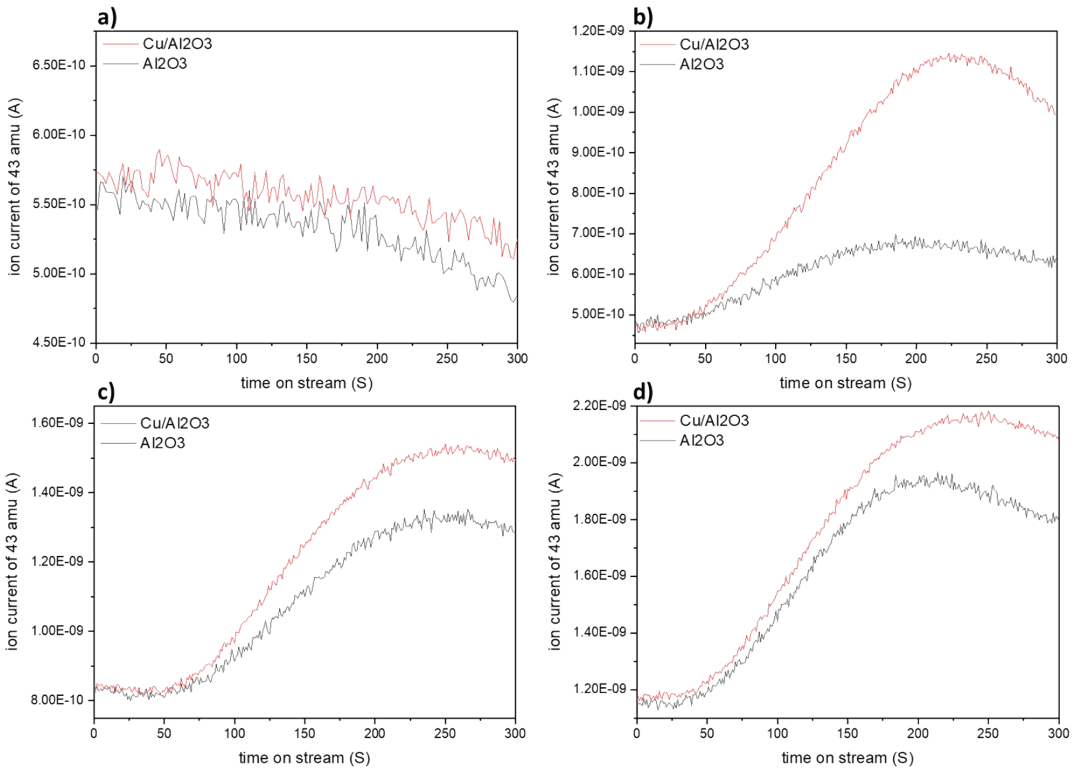

Figure S1. The base-line normalized ion current of the 43 amu corresponding to the concentration of acetylacetone in the PCVD reactor outlet for experiment temperature of a) 140°C, b) 150°C, c) 160°C, and d) 170°C. The drastic increase of ion current at 150°C suggests that the copper particles catalyze the reaction between $Zn(acac)_2$ and hydrogen, leading to preferential deposition of zinc on the copper phase. In contrast, the ion current increase in the case of pristine Al_2O_3 is insignificant due to the lack of catalyst. However, the ion current increase at higher temperatures suggests that the zinc deposition on pristine Al_2O_3 is likely, and the temperatures above 150°C should be avoided for PCVD of zinc on copper.

Figure S2

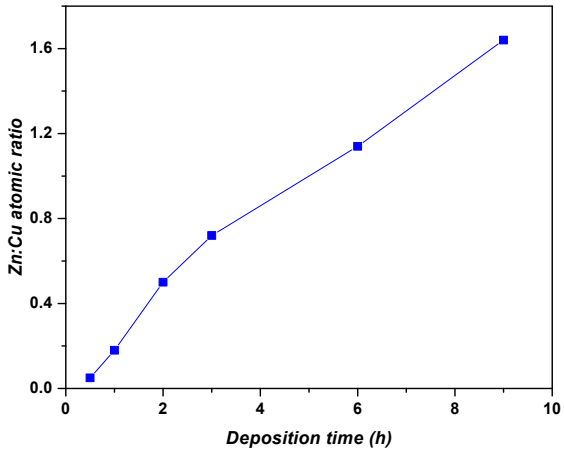

Figure S2. Zinc to copper atomic ratio as a function of zinc deposition time.

Figure S3

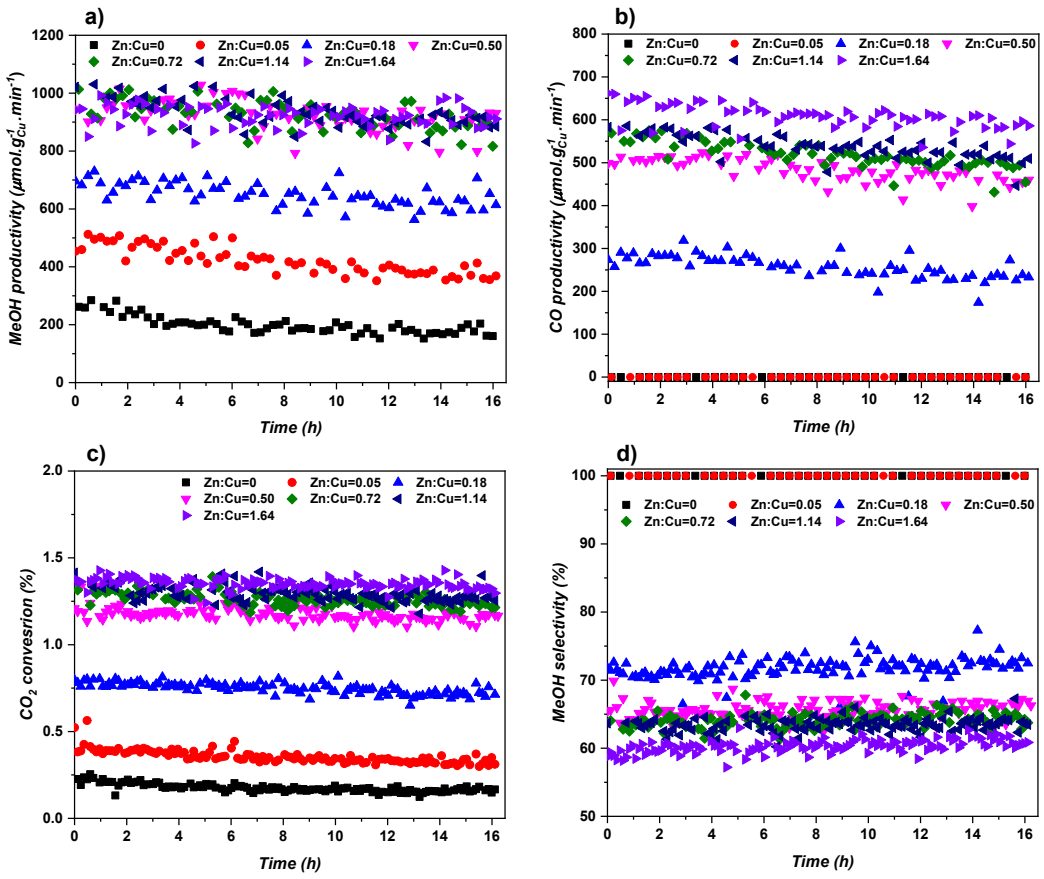

Figure S3. Carbon dioxide hydrogenation activity of samples synthesized with preferential chemical vapor deposition as a function of reaction time; a) methanol productivity, b) carbon monoxide productivity, c) carbon dioxide conversion, and d) methanol selectivity. Activity and selectivity during carbon dioxide hydrogenation were measured under steady-state operation (i.e. after the reaction was carried out for 3 hours before measurements).

Figure S4

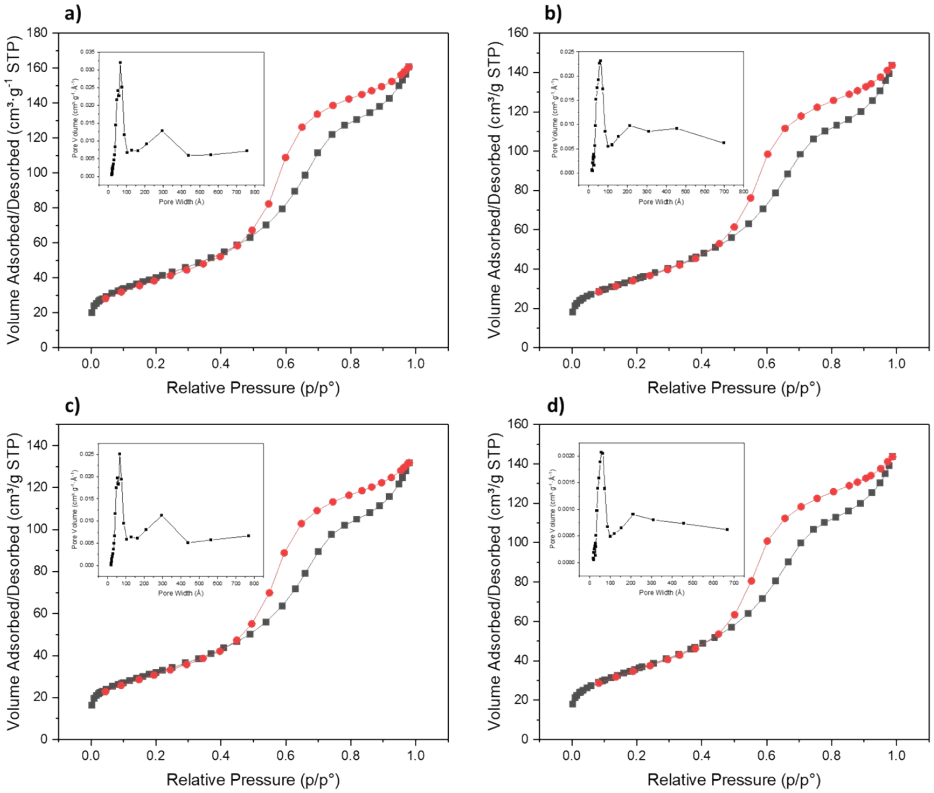

Figure S4. The nitrogen adsorption/desorption isotherms and pore size distribution curves (inset) of a) pristine Al_2O_3, b) CA, c) PCVD, and d) IMP samples, obtained using BET measurement.

Figure S5

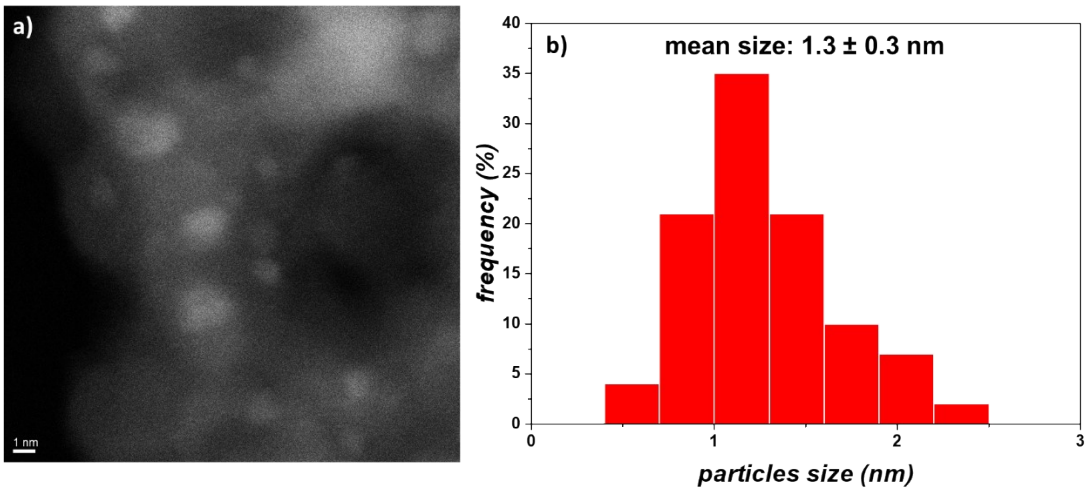

Figure S5. The HAADF-STEM image (a) and copper particle size distribution (b) for CuO/Al_2O_3 synthesized with incipient wetness impregnation.

Figure S6

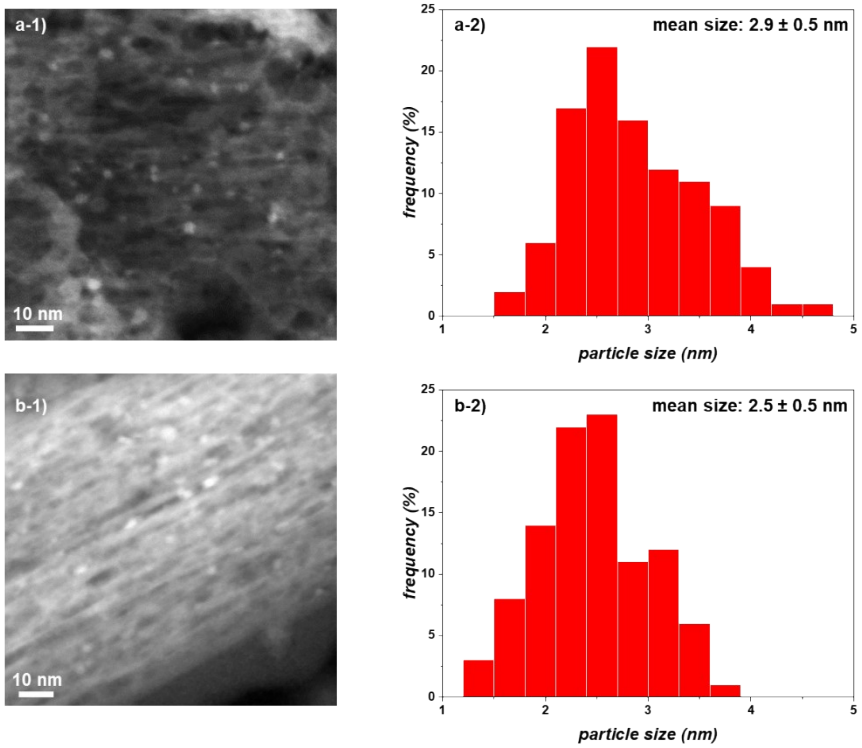

Figure S6. The HAADF-STEM image and the particle size distribution of ZnO-CuO: a) PCVD and b) IMP samples.

Figure S7

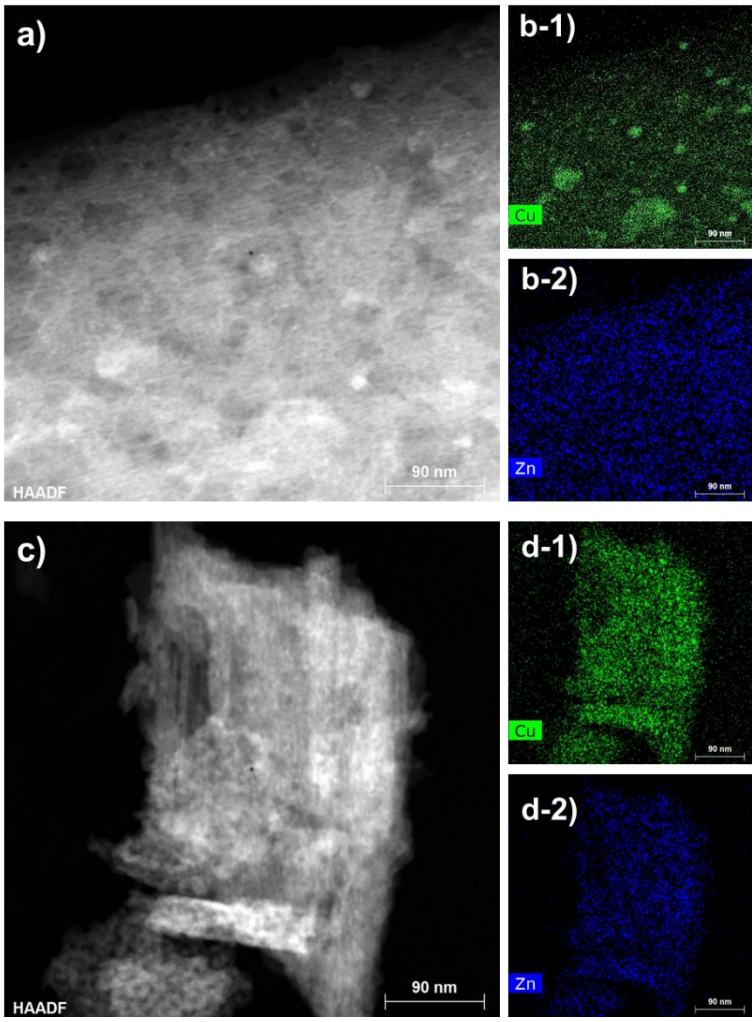

Figure S7. HAADF-STEM images of fresh ZnO-Cu/Al_2O_3 catalysts synthesized with PCVD (a) and IMP (b) methods and the corresponding elemental mappings of copper (b-1 and d-1) and zinc (b-2 and d-2) in these samples.

Figure S8

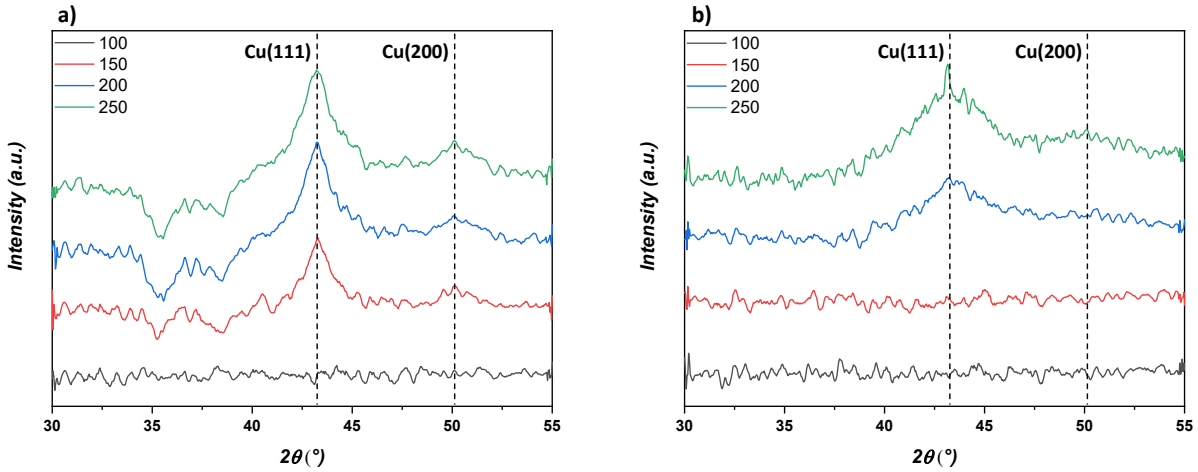

Figure S8. I*n-situ* XRD patterns of ZnO/Cu/Al_2O_3 catalysts after subtraction of pattern obtained at 50°C, synthesized by a) preferential chemical vapor deposition and b) successive incipient wetness impregnation methods during pretreatment with 20 vol. % of hydrogen in helium. The dashed lines indicate the position of copper (111) and (200) reflections.

Figure S9

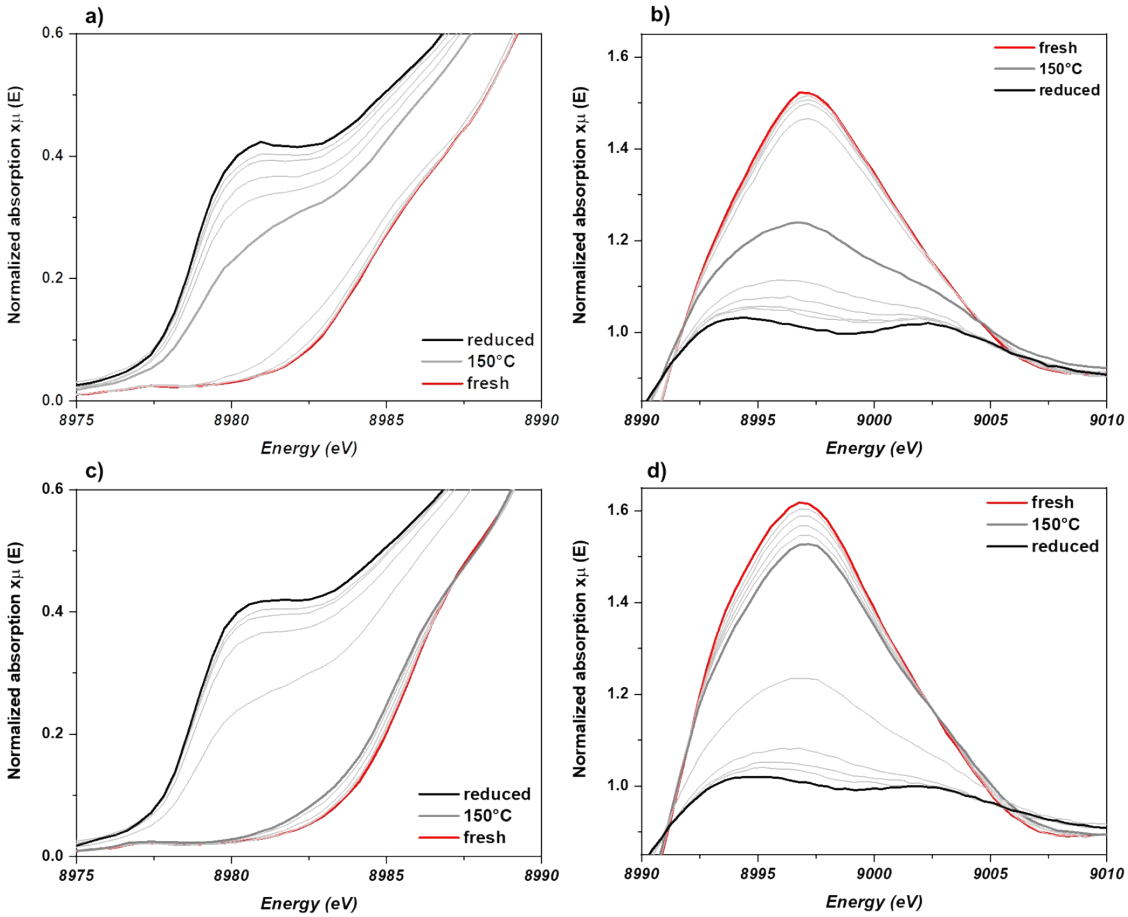

Figure S9. The details of the normalized *in-situ* copper *K*-edge XANES spectra: a) pre-edge and b) white line features of PCVD sample, and c) pre-edge and d) white line features of IMP sample during temperature programed reduction. The red curves were derived from the fresh catalyst at ambient temperature, and the black curves were obtained after 1 hour reduction under 25 vol. % of hydrogen in helium flow at 250°C. The grey curves show intermediary spectra taken at 25°C intervals within this temperature range.

Figure S10

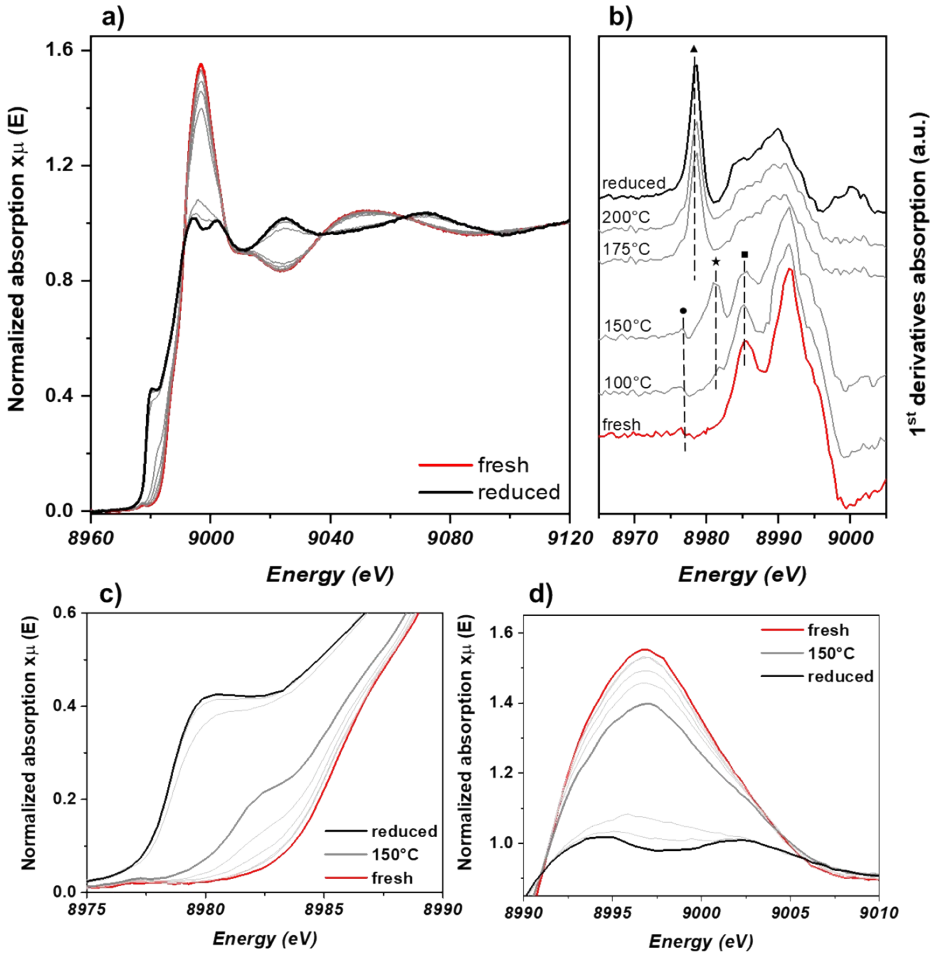

Figure S10. a) Normalized *in-situ* copper *K*-edge XANES spectra of Cu/Al_2O_3 obtained during temperature programed reduction, b) corresponding XANES first derivative, c) pre-edge of XANES spectra, and d) white line of XANES spectra. The red curves were derived from the fresh catalyst at ambient temperature, and the black curves were obtained after 1 hour reduction under 25 vol. % of hydrogen in helium flow at 250°C. The grey curves show intermediary spectra taken at 25°C intervals within this temperature range. Triangle: edge position of Cu^0, Circle: position of pre-edge peak, Square: *1s-4p* transition with shakedown contributions in tetragonal Cu^{2+}, Star: edge position of Cu^{1+}.

Figure S11

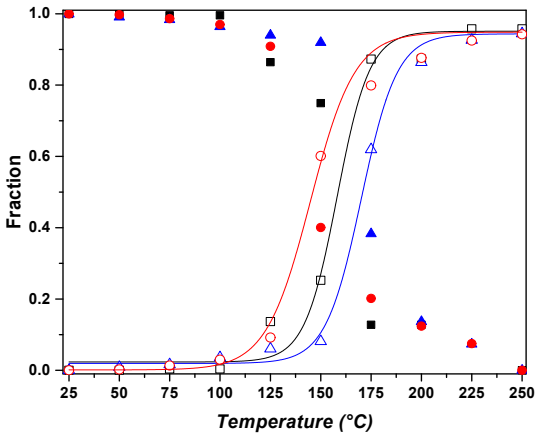

Figure S11. Results of PCA/LCF analyses of the Cu *K*-edge XANES obtained in each of the three catalysts studied during TPR under 25 vol. % hydrogen flow in helium. Filled symbols = Cu^{2+}; open symbols = Cu^{0}. Black = CA; red = PCVD; blue = IMP. In each case the lines fitted to the data are only to guide the eye. The errors in concentrations returned from PCA and LCF analysis is ± 1% in all cases.

Figure S12

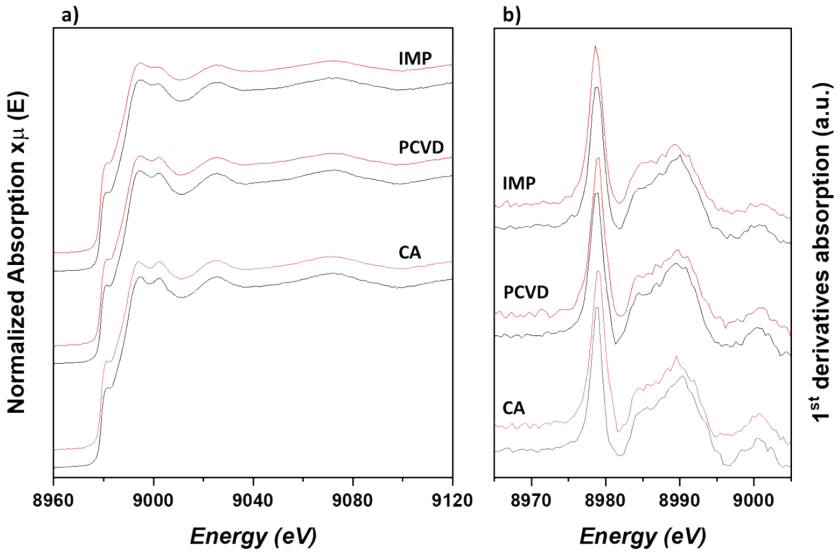

Figure S12. Normalized *in-situ* copper *K*-edge XANES spectra (a) and corresponding XANES first derivatives (b) derived from reduced CA, PCVD, and IMP catalysts (at 250°C under 25 vol. % of hydrogen in helium); before (black) and after pressurizing to 15 bar (red).

Figure S13

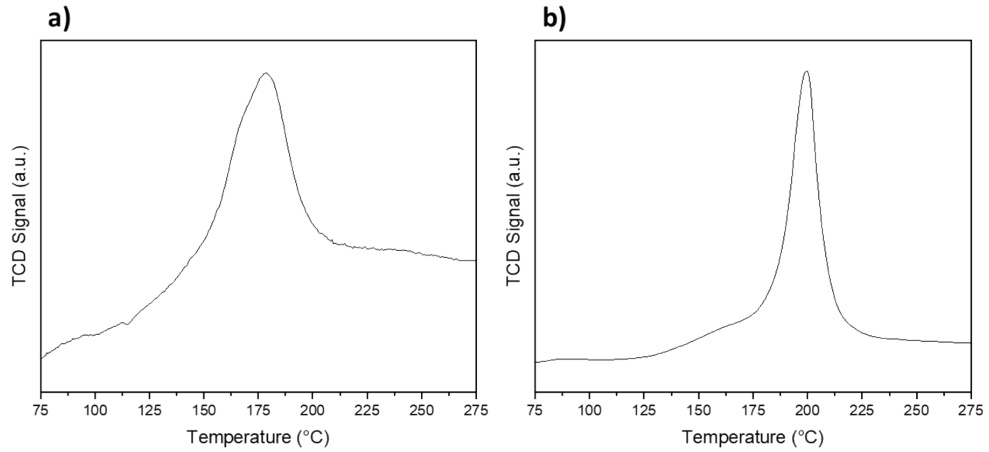

Figure S13. The H_2-TPR experiment for a) PCVD and b) IMP samples.

Figure S14

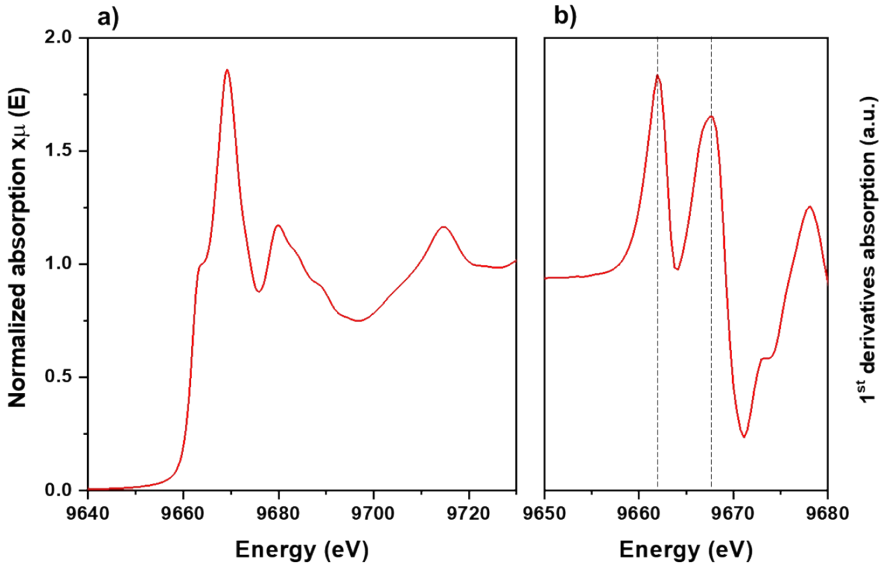

Figure S14. a) Normalized zinc *K*-edge XANES spectra and b) corresponding first derivative of wurtzite zinc oxide; the main peak and shoulder of wurtzite zinc oxide are marked with dashed lines in first derivative.

Figure S15

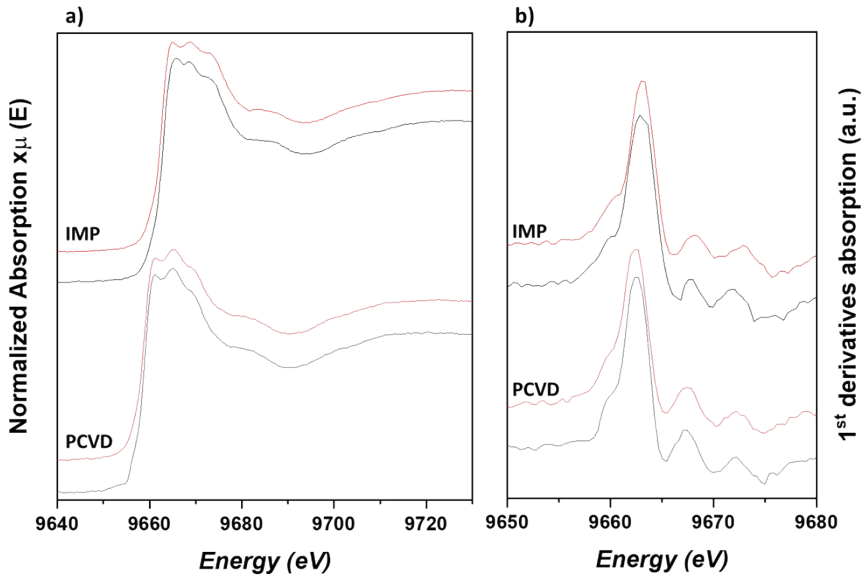

Figure S15. Normalized *in-situ* zinc *K*-edge XANES spectra (a) and corresponding XANES first derivatives (b) derived from reduced PCVD and IMP catalysts (at 250°C under 25 vol. % of hydrogen in helium); before (black) and after pressurizing to 15 bar (red).

Figure S16

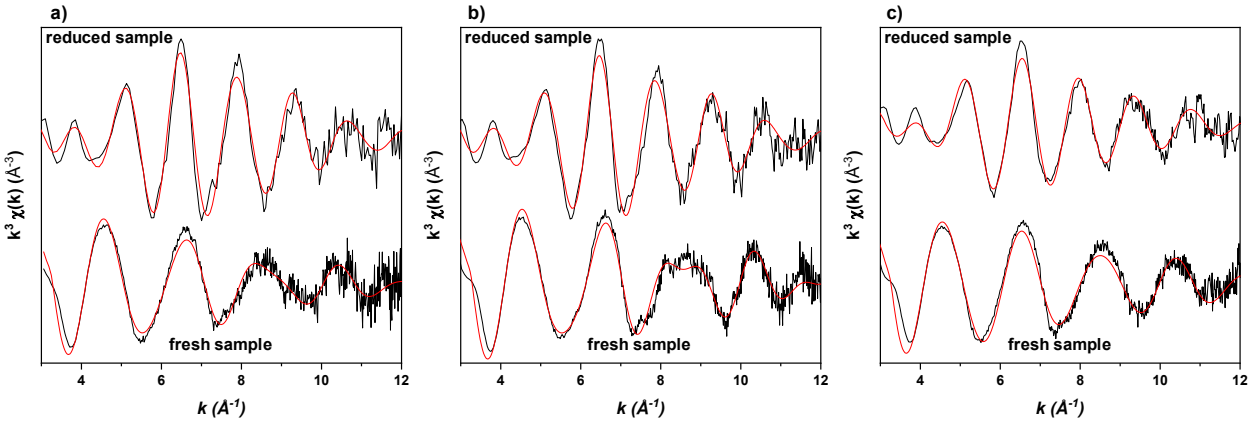

Figure S16. The k^3-weighted copper *K*-edge EXAFS derived from a) CA, b) PCVD, and c) IMP catalysts, for the fresh (ambient temperature) and reduced (250°C for 1 hour under 25 vol. % of hydrogen in helium). Black lines: experiment and red lines: theoretical fits.

Figure S17

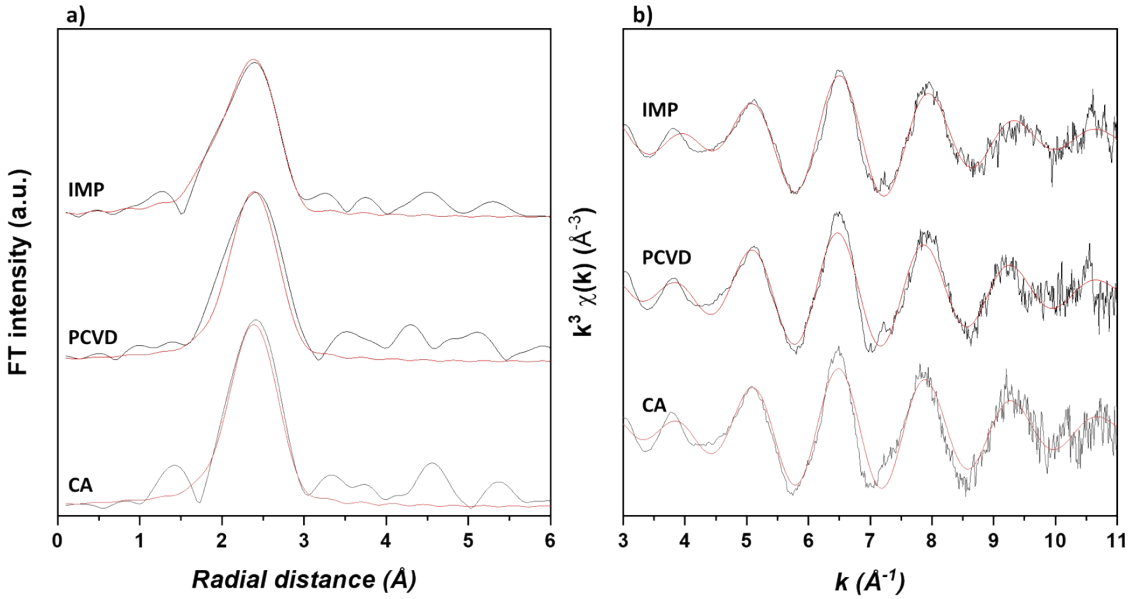

Figure S17. The Fourier transforms (a) and k^3-weighted copper *K*-edge EXAFS (b) derived from CA, PCVD, and IMP catalysts; pressurized to15 bar after reduction (at 250°C under 25 vol. % of hydrogen in helium). Black lines: experiment and red lines: theoretical fits.

Figure S18

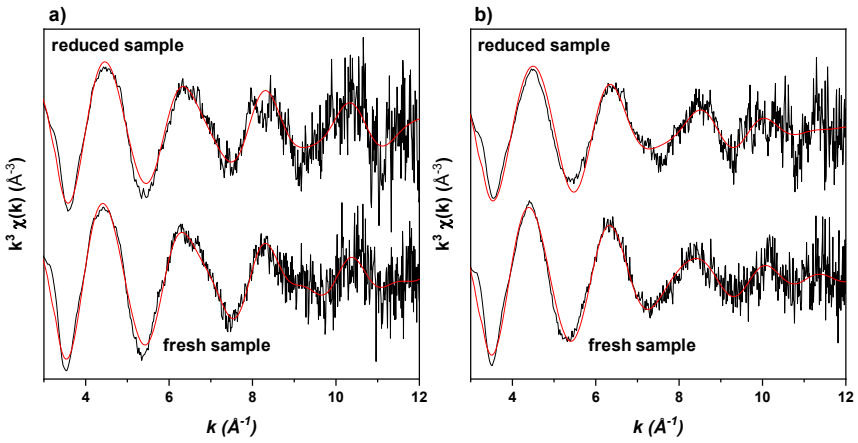

Figure S18. The k^3-weighted zinc *K*-edge EXAFS derived from a) PCVD and b) IMP catalysts, for the fresh (ambient temperature) and reduced (250°C for 1 hour under 25 vol. % of hydrogen in helium). Black lines: experiment and red lines: theoretical fits.

Figure S19

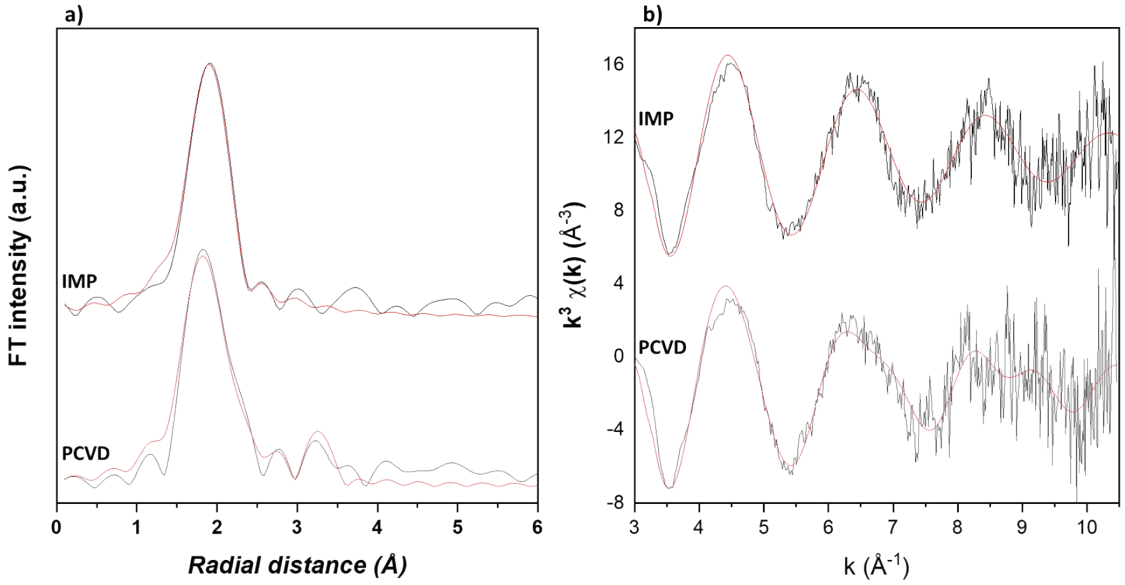

Figure S19. The Fourier transforms (a) and k^3-weighted zinc *K*-edge EXAFS (b) derived from PCVD and IMP catalysts; pressurized to15 bar after reduction (at 250°C under 25 vol. % of hydrogen in helium). Black lines: experiment and red lines: theoretical fits.